Control Factors of Organic Matter Enrichment in Alkaline Lacustrine Source Rocks: A Case Study of the Late Paleozoic Fengcheng Formation in Junggar Basin, NW China

HUANG Renda[1, 2], JIANG Fujie[1, 2, *], HU Tao[1, 2], CHEN Di[1, 2], HUANG Liliang[3], LIU Zheyu[1, 2], WANG Xiaohao[1, 2], ZHANG Chenxi[1, 2], LV Jiahao[1, 2] and WU Yuping[1, 2]

[1] *State Key Laboratory of Petroleum Resources and Prospecting, China University of Petroleum (Beijing), Beijing 102249, China*
[2] *College of Geosciences, China University of Petroleum (Beijing), Beijing 102249, China*
[3] *Research Institute of Petroleum Exploration and Development, Xinjiang Oilfield Company, CNPC, Karamay, Xinjiang 834000, China*

Abstract: The Late Paleozoic Fengcheng Formation shale (LPF shale) in Junggar Basin, NW China, is the oldest alkaline source rocks discovered in the world, which provides a unique perspective for exploring organic matter (OM) enrichment in alkaline lake environment. Combined with the organic carbon isotope profile and paleoenvironment proxies, this study reveals that the LPF shale was deposited in an arid climate with high salinity and strong reductive environment, accompanied by frequent volcanic activities. High TOC values are concentrated in two intervals with frequent fluctuations in OM types. A negative excursion due to changes in sedimentary OM source is found in $\delta^{13}C_{org}$ profile. The excursion corresponds to the OM enrichment interval and accompanied by abnormally high values of Sr/Ba and Sr/Cu. This implies that the extreme arid climate has led to high salinity, resulting in strong reducibility and changes in paleontological assemblages, which in turn controlled the differential enrichment of OM. The Fengcheng Fm. high-quality source rocks are the result of the combined action of climate events, volcanism, high-salinity water environment, and superior hydrocarbon-generating organisms. The results provide new insights into the formation conditions of terrestrial alkaline high-quality source rocks and control factors of alkaline OMs enrichment.

Key words: organic matter enrichment, control factors, alkaline lake source rocks, Fengcheng Formation, Junggar Basin

E-mail: jiangfj@cup.edu.cn

1 Introduction

Alkaline lake (Soda Lake) is a type of high pH lake with high salinity (Jones and Grant, 2000). The alkaline lacustrine deposits have been discovered many times in the world, such as American Green River Formation (Sarg et al., 2013), Australian Observatory Hill Formation (White and Youngs, 1980), Turkey Hirka Formation (Helvacı, 1998), Chinese Hetaoyuan Formation (Su et al., 2020) and Fengcheng Formation (Guo et al., 2021), etc. These alkaline lacustrine deposits all exhibit superior hydrocarbon-generating capacity and are considered to be high-quality source rocks. The late Paleozoic Fengcheng Formation shale (LPF shale) in Junggar Basin, NW China, is the oldest alkaline lacustrine source rock discovered in the world (Cao et al., 2020), providing a unique perspective for exploring the organic matter (OM) enrichment in the alkaline lacustrine source rocks (Guo et al., 2021; Tang et al., 2021). The LPF shale is the main source rock in Mahu Sag, providing a large number of hydrocarbons for Triassic conglomerate tight oil reservoirs and shallow conventional reservoirs (Zhi et al., 2019; Gao et al., 2020; Tang et al., 2021). Moreover, the LPF shale has also shown great potential for shale oil exploration potential recently, and has become a research focus of unconventional petroleum resources (Hu et al., 2021; Li et al., 2021; Tang et al., 2021). Previous studies have shown that the LPF shale have the characteristics of high oil-gas ratio and high hydrocarbon generation (Cao et al., 2020; Zhi et al., 2021). However, the viewpoints on the OM enrichment of Fengcheng Formation (Fm.) high-quality source rocks have not yet been unified. Some studies believe that the alkaline lake background generates a relatively single biological composition and high primary productivity, which in turn led to the enrichment of OM and strong hydrocarbon generation capacity (Cao et al., 2020; Hou et al., 2022). Some others believe that the high salinity water environment creates good preservation conditions and less dilution rather than high primary productivity, therefore the LPF shale exhibits superior hydrocarbon generation potential (e.g., Gao et al., 2020). The differential enrichment process of OM in the LPF shale remains controversial, which greatly restricts the theoretical development of alkaline lacustrine shale OM

enrichment.

Carbon isotopes are considered to reflect changes in global carbon cycle and are widely used in paleoclimate recovery and isochronous comparison of global climate events (Cramer and Jarvis, 2020; Pieńkowski et al., 2020). The carbon in sedimentary OM mainly comes from the photosynthetic fixation of atmospheric and water-dissolved CO_2 by primary producers and the decomposition of carbon-containing compounds, etc. (Zhang et al., 2020). Due to the different carbon sequestration processes of different organisms, there are corresponding differences in their carbon isotopic compositions (Tobin et al., 2021). Therefore, organic carbon isotope composition reflects both atmospheric CO_2 information and sedimentary OM sources. Here, we present a high-resolution comprehensive evolution profile of minerals, geochemical parameters, and organic C-isotope of the LPF shale in MY1 to explore the co-evolution of paleoenvironment and alkaline lacustrine OM deposition. This study finds a correlation between negative organic C-isotopes excursion and OM enrichment interval, and provides new insights into the formation conditions of terrestrial alkaline high-quality source rocks and control factors of alkaline organic matters enrichment under climate evolution background during the Late Paleozoic.

2 Geological Setting

The Junggar Basin is a large-scale oil-producing basin located in northwestern China (Fig.1b; Cao et al., 2015; Cao et al., 2020). During the Late Paleozoic, the Junggar Basin was located within central Siberia at middle-high northern latitudes (~40°N; Fig.1a; Sengor et al., 1993; Wan et al., 2010). Intense collisions in the surrounding area resulted in the boundary faults' deformation, leading to the formation of the basin (Chen et al., 2016). The southeastward marine regression during the Late Paleozoic left a closed ocean in the western Junggar Basin, providing a favorable sedimentary environment for OM preservation (Gao et al., 2020). The Mahu Sag located in the northwest of Junggar Basin is one of the main hydrocarbon-generating sags in the basin (Zhi et al., 2019). Mahu Sag is a post-orogenic extensional fault sag, with a set of delta-lake sedimentary systems developed as a whole (Cao et al., 2020). Mahu Sag is developed on the Carboniferous marine basement and filled with terrigenous strata that consist of the Late Paleozoic Jiamuhe Fm., Fengcheng Fm., Xiazijie Fm., Lower Wuerhe Fm., Upper Wuerhe Fm., Triassic Baikouquan Fm., Karamay Fm., and Baijiantan Fm. (Tang et al., 2021a).

Fengcheng Fm. develops high quality lacustrine source rocks, which are the main hydrocarbon source in Mahu Sag and even the oldest terrestrial shale discovered in China (Yang et al., 2019; Zhi et al., 2021). The Fengcheng Fm. is a set of fine-grained sediments deposited in an alkaline lake environment, which is mainly composed of a mixture of near-source clastic minerals, chemical crystalline materials, and peripheral volcanic materials (Zhi et al., 2019). The Fengcheng Fm. can be divided into Member 1, 2, and 3 from bottom to top. Through MY1 core observation, the member 1 (F_1) mainly develops basalt and tuff, with thin interbedded shale; the member 2 (F_2) and the lower part of member 3 (F_3) is dominated by shale and calcareous shale interbeds; the upper part of member 3 has a coarser grain size overall, and mainly consist of interlayers of fine sandstone and mudstone (Fig.1d). Alkaline minerals such as trona ($Na_2CO_3.NaHCO_3.2H_2O$), nahcolite ($NaHCO_3$), shortite ($Na_2Ca_2(CO_3)_3$), wegscheiderite ($Na_5H_3CO_3)_4$) are widely developed in the shale interval, indicating a strongly evaporative alkaline lake environment (Fig.2; Yu et al., 2018; Gao et al., 2020). Moreover, the LPF shale is rich in hydrocarbons. The phenomenon of oil stain and fractures filled by hydrocarbons can be seen clearly by naked eyes and fluorescence (Lv et al., 2023). In general, the LPF shale is deposited in a stable lake environment and has excellent exploration potential for shale oil resources.

3 Data and Methods

In this study, 481 core samples were obtained from the LPF shale (4580–4860m) in well MY1, with the average sampling interval of 0.9m (Fig.1c, d). The lithology of samples are mostly shale and calcareous shale. Among them, 137 core samples were evenly selected and ground to 200 mesh for X-Ray Diffraction analysis. A D2 Phaser diffractometer was used to perform X-Ray diffraction on mineral powders and compare with the standard mineral diffraction pattern to obtain the content of various minerals in the samples. 481 sample powders were heated in a water bath with 3mol/L hydrochloric acid to remove inorganic carbon. After rinsed to neutrality, the powders were fed into LECO CS230 carbon-sulfur analyzer for Total Organic Carbon (TOC) testing and Rock-Eval 6 Pyrolyzer for Rock Pyrolysis (Peters, 1986). In rock pyrolysis, the initial temperature set to 300℃ and heated to 600℃ at a rate of 50℃/min to determine free hydrocarbons (S_1), pyrolyzed hydrocarbons (S_2) and the temperature corresponding to the highest hydrocarbon yield (T_{max}) (Espitali E et al., 1977; Espitali E et al., 1984). A parallel sample was added for every 15 samples, and the uncertainty was within 0.1%. 90 samples were tested for organic carbon isotopes using a Thermo Scientific (thermoelectric) FLASH HT EA-MAT 253 IRMS. The sample depths ranged from 4577.67m to 4754.8m, with the average sampling interval of 1.99m. The standard material is IAEA-600 Caffeine, USG24 Graphite. The results adopt the PDB standard, and the uncertainty was within 0.2‰. The thin section observation and fluorescence macerals

were observed using a Leica microscope. The content of major and trace elements were measured using a Bruker S1 TITAN 800 handheld XRF spectrometer. During the test, the sample was irradiated by X-ray to emit the secondary X-ray. The element type was identified by the wavelength and energy of the secondary X-ray, and the quantity of elements was measured by the ray density. The measuring accuracy is 1ppb, and the measurement errors of different elements are as follows: Ba 5%; Fe, S 0.5%; Sr, Mo, Cu,Hg 2ppb. All tests and microscopic observation were conducted at China University of Petroleum (Beijing).

4 Results

4.1 Mineral composition

XRD mineral analysis shows that the LPF shale is mainly composed of quartz, feldspar, calcite, and dolomite, with low clay minerals content (Fig.2; Fig.3). Pyrite is visible in the whole section. The mineral composition is characterized by rapid changes and periodic fluctuations. The distribution of quartz and feldspar content ranges from 6.9% to 89.1%, with an average of 46.8%. The clay minerals content averages 10.7%. The carbonate mineral content ranges from 3.2% to 92.3%, with an average of 35.9%. Among them, calcite accounted for an average of 14.0%, and dolomite for 26.8%. Core observation shows that alkaline minerals are developed in Fengcheng Fm., especially in F_2. In summary, the LPF shale is the common result of weathering transport sedimentation and chemical sedimentation, and terrigenous clastic sediments predominate.

4.2 Geochemical characteristics

The characteristics of 481 samples show that the TOC is distributed between 0.06% and 2.85%, with an average of 0.65%; the total hydrocarbon content (sum of S_1 and S_2) was distributed between 0.12 and 15.41mg HC/g Rock, with an average of 2.67 mg HC/g Rock (Fig.4a). According to the evaluation standard (Tissot and Welte, 1984; Hu et al., 2022a), the LPF shales are of good quality, and most of them reach the standard of fair source rock (Fig.4a).

T_{max} can be used to evaluate the thermal maturity of OM (Tissot and Welte, 1984; Hu et al., 2022b). However, the bitumen or intrusion of oil-based mud may produce a 'contamination' of kerogen and cause T_{max} suppression (Zhang et al., 2006; Hu et al., 2021; Katz and Lin, 2021). After removing the 'contamination', the T_{max} of the LPF shale ranges from 401–458℃, with an average of 436℃ (Fig.4b), indicating it is currently in the early-mature to mature stage. The hydrocarbon index (HI, $HI=100\times S_2/TOC$) represents the relative hydrogen content in OM, HI-T_{max} chart is suitable for OM type classification in immature-mature stage (Tissot and Welte, 1984). Commonly, the hydrocarbon-generating parent materials of sapropelic OM (type I) are mainly lake organisms such as algae and bacteria with high hydrogen content, more aliphatic straight-chain compounds, showing strong oil-generating capacity. Humic OM (type Ⅲ) are mainly derived from terrestrial higher plants with more aromatic branched-chain compounds and is more inclined to produce gas. The sapropel-humus type (type II_1) and the humic-sapropiate type (type II_2) are in between (Ding et al., 2017; Hu et al., 2022c). The chart shows that the OM is mainly typed II_2 in the LPF shale, with the contribution of algae and the input from terrestrial higher plants (Fig.3).

4.3 Organic carbon isotopes

The distribution of $\delta^{13}C_{org}$ values ranges from -21.87‰ to -29.48‰ with obvious fluctuations in the LPF shale. 2 negative carbon isotope excursions (NCIE) can be identified in the $\delta^{13}C_{org}$ profile (Fig.3). NCIE 1 deviates from -26.36‰ to -29.48‰, including the minimum value of the entire profile. NCIE 2 shows a trend of excursion from -25.3‰ to -28.1‰, with multiple negative excursion points and fluctuation in carbon isotopes. Overall, the 2 NCIEs were characterized by slow negative excursion and slow return. In addition, $\delta^{13}C_{org}$ showed a clear lightening trend as TOC increased (Fig.4c).

4.4 Organic matter occurrences

Under the fluorescence microscope, the features of different OM types can be clearly observed. Type II_1 mainly develops spherical algae and retains their original form (Fig.5a, b); while the algae in type II_2 are mainly filamentous algae and develop dispersedly (Fig.5c, e). Besides, a large area of dark yellow fluorescence can be seen in the field of view, which is a mixture of small-scale inorganic minerals and OM formed by bacteria breaking down OM (Fig.5g; Ma et al., 2020). Vitrinite and inertinite can be seen under the microscope (Fig.5e, f, g, h), which are often derived from terrestrial higher plants and retain the original plant structure. Pyrite is visible under reflected light (Fig.5b, d, f, h).

4.5 Content of elements

Due to the variable depositional processes of different sedimentary systems, there is no universal proxy and threshold that can absolutely indicate the paleo redox environment (Algeo and Rowe, 2012). Therefore, the discusstion of paleo redox should be based on local succession and use multiple proxies

to reduce uncertainty (Algeo and Liu, 2020). C-S-Fe three-terminal diagram has been widely used in the restoration of paleo redox environment in sediments (Dean and Arthur, 1989; Arthur and Sageman, 1994). According to the C-S-Fe three-terminal diagram, S/Fe can be used to evaluate paleo redox environment (Dean and Arthur, 1989; Peng, 2022). The concentration of Mo element in sediments usually occurs in strongly reducing water environments (Algeo and Tribovillard, 2009; Tribovillard et al., 2012). In a strongly reducing environment, the water-soluble MoO_4^{2-} reacts with sulfide to form $MoO_xS_{4-x}^{2-}$ which is easily absorbed on the surface of OM and further to preserve in sediments (Tribovillard et al., 2004; Algeo and Tribovillard, 2009). Hence, Mo is sensitive to redox and can be used to evaluate paleo redox environment. Sr element tends to be enriched in arid environment, while Cu element prefer to be enriched in humid environment, so Sr/Cu proxy is widely used in paleo climate restoration (Lerman, 1978). With 10 as the threshold, Sr/Cu<10 indicates a warm and humid climate, while Sr/Cu>10 indicates an arid and hot climate (Lerman, 1978). Sr/Ba is a good indicator of paleo salinity due to the difference migration ability of the two elements (Wei and Algeo, 2020). Based on the study of Chivas et al. (1985), the thresholds of Sr/Ba for freshwater, brackish, and saline lacustrine deposits were determined to be 0.5 and 1.0. The abnormal high concentration of Hg in sediments are usually caused by the significant release of Hg by volcanic eruptions (Grasby et al., 2013; Percival et al., 2017). Thus, Hg concentration can be used as a proxy for volcanic activities.

The S/Fe distribution of the LPF shale ranges from 0.02 to 3.12, with an average of 0.81 (Fig.6b). Compared with the Cline marine shale in the Midland Basin, America (0.04–0.94; Peng, 2022), the S/Fe distribution of the LPF shale is generally higher. Despite there are local influence of different depositional system, the LPF shale has been shown to be deposited in a more reductive water environment than the Cline shale. Mo element is widely detected in the LPF shale. The content of Mo distributes in 0–315ppm, with an average of 15.50ppm (Fig.6c). Sr/Cu ranges from 1.66 to 116.14, with an average of 11.56; Sr/Ba distributes in 0.14–9.98, with an average of 1.40 (Fig.6d and e). The two proxies both indicate that the LPF shale was deposited in a saline water environment in an arid climate. Three abnormal concentrations of Hg were detected in the LPF shale which are distributed at depth of 4602.59m, 4632.43m, and 4726.85m, may be indicative of volcanic activities (Fig.6f).

5 Discussions

5.1 Paleoenvironment variation

Pyrite is widely developed in the LPF shale, containing framboids and euhedral crystals (Fig.3; Fig.6a). The framboidal pyrite is formed near the redox interface and fell into sediments after crystallization (Berner, 1984). Thus, its presence in sediments is an indicator of reducing environment. However, when the redox interface is in sediments, the framboidal pyrite would has a larger particle size due to the support of sediments (Wilkin et al., 1996). The abundant and extensive small grain size framboidal pyrites indicate a reducing water environment during the LPF shale sedimentary period (Fig.6a; Jones and Manning, 1994; Shevelkova et al., 1996; Zhou and Jiang, 2009). Moreover, the consistent variation of S/Fe and Mo values further confirmed that the LPF shale was deposited in a reducing water environment (Fig.6b and c). The development of alkaline minerals and high Sr/Cu and Sr/Ba values indicate that the LPF shale was deposited in a strong evaporation environment with high salinity in an arid-semiarid climate (Fig.2; Fig.6d and e). The LPF shale was a mixture of terrigenous detritus and calcium chemical deposition. The terrigenous detritus shows the characteristics of high quartz and feldspar content and low clay minerals content. To the top of LPF shale (4580–4590m), clay minerals dominated terrigenous detritus, which may imply the change of provenance. Meanwhile, in this interval, the climate turned to humid, the water body limitation was reduced, the salinity decreased and changed into an oxidizing environment. Due to the limitation of experimental accuracy, this study failed to establish an Hg variation profile of ppb level. However, the three anomaly concentrations of Hg can indicate volcanic activities to some extent (Fig.6f). In addition, previous studies have reported numerous zircon U-Pb ages from the Fengcheng Fm., showing that volcanic activity was frequent in the around of Mahu Sag during the LPF shale depositional period (Liu et al., 2019; Tang et al., 2021b; Wang et al., 2021; Wang et al., 2022). The frequent volcanic activity brought a lot of nutrients and alkali-forming substances to the lake, which further led to the development of alkaline lake (Cao et al., 2020; Guo et al., 2021). During the period, the LPF shale developed an arid-semiarid climate. Increased evaporation from water bodies in the limited lake basin led to reducing water storage reduction and increasing salinity, and the supersaturated alkaline substances precipitated. The climate variation regulated the salinity and limitations of water bodies and thus controlled the redox conditions. The paleo redox proxies and TOC values show consistent fluctuation, indicating that the reducibility of water environment is an important factor affecting the enrichment of OM.

5.2 Carbon cycle perturbation

The hydrocarbon-generating organisms of the LPF shale are mainly primary producers such as bacteria and algae, also include pollen and unknown organisms composed of elemental sulfur (Cao et al., 2020;

Guo et al., 2021). Photosynthetic carbon sequestration by primary producers can reflect changes in atmospheric CO_2 (Hayes et al., 1999; Kump and Arthur, 1999). In this study, the $\delta^{13}C_{org}$ profile exists 2 negative excursions, NCIE 1 at 4697–4708m and NCIE 2 at 4621–4644m (Fig.7b).

NCIE 1 manifests as a strong negative excursion after a brief positive excursion. It has the same characteristics as the negative excursion in several terrestrial and marine profiles in the world (Fig.7c, d; Buggisch et al., 2011; Lu et al., 2021). The OM type remains relatively stable in this interval, which excluded the effect of paleontological assemblage changes on $\delta^{13}C_{org}$. Wang et al. (2022) reported a NCIE with similar characteristics in Fengcheng Fm. integrated $\delta^{13}C_{carb}$ profile is likely to be coupled with this event (Fig.7a). Through astrochronology analysis and global correlation of $\delta^{13}C$ profiles in Huang et al. (2023), NCIE 1 was identified as a global response to changes in global atmospheric CO_2 composition. Lu et al. (2021) also interpreted the NCIE as a global change in atmospheric CO_2 caused by volcanism in North China Plate, Tarim Plate, and the formation of Skagerrak-Centered Large Igneous Provinces. The frequent volcanic activities in a short period released a large amount of mantle-derived CO_2 into atmosphere, resulting in a shift in atmospheric CO_2 isotope composition to light carbon (Saunders, 2005). Climate anomalies caused by volcanic activities affected runoff input and monsoon intensity, reducing lake limitations, and increasing water storage. After the volcanic activities, atmosphere CO_2 gradually returned to normal, the climate returned to stability.

No records similar to NCIE 2 were found in published $\delta^{13}C$ profiles or in the Fengcheng Fm. $\delta^{13}C_{carb}$ profile (Fig.7). Hence, NCIE 2 is shown to be a regional $\delta^{13}C_{org}$ negative excursion. In this interval, the OM type changes frequently (Fig.2), indicating fluctuations in OM source. Generally, terrestrial primary producers have heavier carbon isotopes because they exhibit stronger ^{12}C fractionation than marine primary producers (Arthur et al., 1985; Tyson, 1995). Lake OM also exhibits a lighter C-isotope composition than terrestrial OM. The overall increase in sedimentary OM (Fig.2) suggests that the NCIE 2 is more likely to derive from the increase of light-carbon-enriched OM rather than the decrease in the heavy-carbon-enriched OM input. There are two possibilities for the increase in the proportion of ^{12}C-enriched OM in sedimentary OM. The first is changes in the proportions of terrestrial and lake-sourced OM in deposits. It may be the environmental changes that caused the increase of nutrients in the water, which further leads to the overall prosperity of aquatic organisms resulting in increased burials, and ultimately manifested as the enrichment of light carbon. Another possible explanation is the carbon isotope composition of lake living organisms has changed, with some kind of light-carbon-enriched organisms occupying the main component. This seems to be more reliable in terms of environmental coupling changes. Heath et al. (2021) suggested the flourishing of chemoautotrophs may be a factor leading to the negative excursion of $\delta^{13}C_{org}$. Modern biological studies have shown that the C-isotope composition of sulfide-oxidizing bacteria in the Black Sea is lighter than that of photosynthetic organisms (Kodina et al., 1996). Cao et al. (2020) reported a kind of unknown organism composed of elemental sulfur existed in the LPF shale, which may be the relevant evidence for the development of chemoautotrophs. Ma et al. (2020) also believed the contribution of special organisms in the LPF shale led to a strong hydrocarbon-generating capacity. The OM type transitioned to type Ⅰ, suggesting that the lake did not receive the dumping input of terrestrial OM at this time, and it was still a limited lake (Fig.3). During this period, Sr/Ba values increased (fig.6e), suggesting a more arid climate. The limited lake basin is greatly affected by climate. The arid climate leads to an increase in water salinity, which further strengthens the reduction degree, corresponding to the increase of Sr/Cu, S/Fe, and Mo. The concentration of Hg in this interval indicates volcanisms, which provided abundant nutrients for the lake. Climate variation has led to changes in water environment, and further led to the succession of paleontological assemblages. The abundance of nutrients allowed special organisms to flourish. During this period, chemoautotrophs may have been fully developed and prosperous, occupying a dominant position. Their increased proportion in lake organisms eventually resulted in the enrichment of light carbon and the excursion of $\delta^{13}C_{org}$.

5.3 Differential enrichment process of LPF shale organic matter

Organic content in rocks is generally controlled by the original amount, degree of thermal evolution and preservation conditions (Li et al., 2021; Fan, 2022; Hu et al., 2022a). During the Fengcheng Fm. depositional period, the high water salinity would cause stratification of the water body, resulting in an anoxic environment at the bottom of lake that is conductive to the preservation of OM (Wang et al., 2020). The vertical stability of T_{max} suggests that the LPF shale has generally experienced the same thermal evolution stage (Fig.2). Thus, the TOC and total hydrocarbon content value can represent the original abundance of source rocks. For source rocks with every different quality, the OM types are relatively concentrated. Good source rocks are more distributed in the upper part of the entire dataset, while poor source rocks are more distributed in the lower part (Fig.4b). Thus, the OM type is indicated to be an important factor for the differential enrichment of OM. TOC and C-isotopes show a clear negative correlation (Fig.4c), furtherly indicating paleontological assemblage differences with TOC changes. It is considered that a kind of basic organism developed throughout the entire depositional period of the LPF shale. The basic organisms are the main contribution of OM at low TOC values that

they have a heavier C-isotope composition and low abundance. In these low TOC intervals, the OM is generally typed II_2 and III, which may be the inferior hydrocarbon-generating organisms in lakes and the higher plants detritus imported with runoff. In the high TOC enrichment interval, a special kind of organism with high hydrocarbon yield developed, which is the main organism and provides abundant original buried OM. The kind of organism with a relatively lighter C-isotope composition is the superior parent material of hydrocarbon-generating. It developed abundantly in a suitable environment, making the sedimentary OM manifests as type I. Vertically, there are two high TOC intervals in the LPF shale in MY1 (4770–4790m and 4610–4640m respectively; Fig.2), which are coupled with the development of type I OM. In addition, in the two high TOC intervals, Sr/Cu shows abnormally high values, and S/Fe and Sr/Ba exhibit relatively high values(Fig.6b, d, e). It is suggested that the extremely arid climate controlled the water environment to high salinity and high reducibility, and further controlled the enrichment of OM. The NCIE 2 corresponds to the second high TOC interval, with a Hg abnormally concentration value (Fig.2). The succession of paleontological assemblage caused by abnormal environmental changes, and the abundant nutrients provided by volcanisms during NCIE 2 may provide a suitable conditions for the superior hydrocarbon-generating organisms to flourish. Since the first interval has similar characteristics to the second interval, it is inferred that the interval might also have a NCIE with similar causes and climate changes to NCIE 2, which would confirm our interpretation.

Consequently, high TOC intervals and other intervals have different enrichment processes (Fig.8). During the development of high TOC intervals, volcanic activity, and high salinity provided rich nutrients and good preservation conditions, which were the basis for the substantial growth of original OM. The superior lake organisms are the important parent material source and the key factor in the development process. Accidently climate events lead to the water environment changes, creating more suitable living conditions for the superior organisms. Their short-term prosperity further controls the enrichment of OM. Climate anomalies may have a contribution from volcanic activities, but their main driving factors still need further investigation. In other periods, there was less original buried OM due to the lack of climate events to drive the development of superior organisms, resulting in lower residual TOC values.

6 Conclusions

In this study, the Late Paleozoic Fengcheng formation (LPF) shale cores from MY1 were taken as the example to conduct systematic analysis and testing. The geochemical characteristics of the LPF shale have been identified and the paleoenvironment changes of the alkaline lake were rough established. This study clarified the control factors of alkaline lacustrine high-quality organic matter enrichment, providing a new insight into the formation of alkaline high-quality source rocks, and is of great significance to continental alkaline lacustrine shale oil exploration.

(1) The late Carboniferous-Early Permian generally developed an arid-semiarid climate. The increase in water evaporation led to the decline of lake level and the increase of salinity in Mahu Sag. Frequent volcanic activities brought a lot of alkaline substances, which controlled the alkaline lake development. The lake is generally a high salinity-reducing environment with a weak hydrodynamic. A set of high-abundance source rocks composed of both terrigenous clastic and chemical precipitations were deposited in this environment.

(2) The LPF alkaline source rock is in the mature stage with a uniform thermal evolution degree. The organic matter ranges from type I to type III, with type II_2 being predominant. The high TOC values are concentrated in two depth intervals of 4770–4790m and 4610–4640m. Through comparative analysis, this study found that the $\delta^{13}C_{org}$ composition and OM type of high TOC intervals and other intervals, which suggests that they have differences in the hydrocarbon-generating organisms. The sedimentary organic matter composition of ordinary source rocks is the inferior hydrocarbon-generating organisms in lake and the higher plant debris input with runoff; while the sedimentary organic matter composition of high TOC intervals is a kind of special superior organisms with strong hydrocarbon-generating capacity in lakes. The existing speculation points to chemoautotrophs.

(3) The formation of the LPF high-quality source rocks is contributed by a coupling of multiple factors. Frequent volcanic activities input a large number of alkaline substances and nutrients into the lake, which not only controls the formation of alkaline lake and high salinity, but also provides the basis for the prosperity of lake organisms. Accidental short-term climatic events affected the aquatic environment, controlled the succession of lake paleontological assemblage, and resulted in relatively single biodiversity. During this period, a kind of superior hydrocarbon-generating organism flourished in the lake, leading to the abundant enrichment of organic matter in alkaline high-quality source rocks.

Acknowledgments

This study was supported by the National Natural Science Foundation of China (Grant Nos. 41872128, 42202133), the Strategic Cooperation Technology Projects of CNPC and CUPB (Grant No. ZLZX2020-01-05). We are grateful to the Xinjiang Oilfield for the support and help with experiments and basic data.

References

Algeo T.J., Tribovillard N., 2009. Environmental analysis of paleoceanographic systems based on molybdenum–uranium covariation. Chemical Geology, 268, 211-225.

Algeo T.J., Rowe H., 2012. Paleoceanographic applications of trace-metal concentration data. Chemical Geology, 324-325, 6-18.

Algeo T.J., Liu J.S., 2020. A re-assessment of elemental proxies for paleoredox analysis. Chemical Geology, 540, 119549.

Arthur M., Dean W., Claypool G., 1985. Anomalous ^{13}C enrichment in modern marine organic carbon. Nature 315.

Arthur M.A., Sageman B.B., 1994. Marine black shales: depositional mechanisms and environments of ancient deposits. Annual Review of Earth and Planetary Sciences, 22, 499-551.

Berner R.A., 1984. Sedimentary pyrite formation: An update. Geochimica Et Cosmochimica Acta, 48, 605-615.

Buggisch W., Wang X.D., Alekseev A.S., Joachimski M.M., 2011. Carboniferous-Permian carbon isotope stratigraphy of successions from China (Yangtze platform), USA (Kansas) and Russia (Moscow Basin and Urals). Palaeogeography, Palaeoclimatology, Palaeoecology, 301, 18-38.

Cao J., Lei D., Li Y., Tang Y., Abramiti, Chang Q.S., Wang T.T., 2015. High-quality source rocks of ancient alkaline lakes: Lower Permian Fengcheng Formation in Junggar Basin. Acta Petrolei Sinica, 36, 781-790.

Cao J., Xia L.W., Wang T.T., Zhi D.M., Tang Y., Li W.W., 2020. An alkaline lake in the Late Paleozoic Ice Age (LPIA): A review and new insights into paleoenvironment and petroleum geology. Earth Science Reviews, 202, 103091.

Chen Z.H., Wang X.L., Zha M., Zhang Y.Q., Cao Y.C., Yang D.S., Wu K.Y., Chen Y., Yuan G.H., 2016. Characteristics and formation mechanisms of large volcanic rock oil reservoirs: A case study of the Carboniferous rocks in the Kebai fault zone of Junggar Basin, China. AAPG Bulletin, 100, 1585-1617.

Chivas A.R., De Deckker P., Shelley J., Michael G., 1985. Strontium content of ostracods indicates lacustrine palaeosalinity. Nature, 316, 251-253.

Cramer B.D., Jarvis I., 2020. Chapter 11 - Carbon Isotope Stratigraphy, In:Gradstein Felix M., Ogg, James G., Schmitz, Mark D., Ogg, Gabi M.(Eds.), Geologic Time Scale 2020. Elsevier, pp.309-343.

Dean W.E., Arthur M.A., 1989. Iron-sulfur-carbon relationships in organic-carbon-rich sequences; I, Cretaceous Western Interior Seaway. American Journal of Science, 289, 708-743.

Ding X.J., Gao C.H., Zha M., Chen H., Su Y., 2017. Depositional environment and factors controlling β-carotane accumulation: A case study from the Jimsar Sag, Junggar Basin, northwestern China. Palaeogeography, Palaeoclimatology, Palaeoecology, 485, 833-842.

Espitali E.J., Laporte L., Madec M., Marquis F., Leplat P., Paulet J., Boutefeu A., 1977. Méthode rapide de Caracterisation des roches mères de leur potentiel pétrolier et de leur degré d'evolution. Rev.inst.francais Du Petrole, 23-42.

Espitali E.J., Makadi K.S., Trichet J., 1984. Role of the mineral matrix during kerogen pyrolysis. Organic Geochemistry, 6, 365-382.

Fan B.J., 2022. Geochemical Characteristics and Paleoenvironment of Organic-Rich Triassic Shale in the Central Ordos Basin. Natural Resources Research, 31, 1739-1757.

Gao Y., Huang H., Tao H.F., Carroll A.R., Qin J.M., Chen J.Q., Yuan X.G., Wang C.S., 2020. Paleoenvironmental setting, mechanism and consequence of massive organic carbon burial in the Permian Junggar Basin, NW China. Journal of Asian Earth Sciences, 194, 104222.

Grasby S.E., Sanei H., Beauchamp B., Chen Z.H., 2013. Mercury deposition through the Permo–Triassic Biotic Crisis. Chemical Geology, 351, 209-216.

Guo P., Wen H.G., Li C.Z., Jin J., Lei H.Y., 2021. Origin and enrichment of borates in a Late Paleozoic alkaline lake-playa deposit, Junggar Basin, NW China. Ore Geology Reviews, 138, 104389.

Hayes J.M., Strauss H., Kaufman A.J., 1999. The abundance of 13C in marine organic matter and isotopic fractionation in the global biogeochemical cycle of carbon during the past 800 Ma. Chemical Geology, 161, 103-125.

Heath M.N., Cramer B.D., Stolfus B.M., Barnes G.L., Clark R.J., Day J.E., Barnett B.A., Witzke B.J., Hogancamp N.J., Tassier-Surine S., 2021. Chemoautotrophy as the driver of decoupled organic and carbonate carbon isotope records at the onset of the Hangenberg (Devonian-Carboniferous Boundary) Oceanic Anoxic Event. Palaeogeography, Palaeoclimatology, Palaeoecology, 577, 110540.

Helvacı C., 1998. The Beypazari trona deposit, Ankara Province, Turkey.

Hou M.G., Qu J.X., Zha M., Swennen R., Ding X.J., Imin A., Liu H.L., Bian B.L., 2022. Significant contribution of haloalkaliphilic cyanobacteria to organic matter in an ancient alkaline lacustrine source rock: A case study from the Permian Fengcheng Formation, Junggar Basin, China. Marine and Petroleum Geology, 138, 105546.

Hu T., Pang X.Q., Jiang F.J., Wang Q.F., Liu X.H., Wang Z., Jiang S., Wu G.Y., Li C.J., Xu T.W., Li M.W., Yu J.W., Zhang C.X., 2021. Movable oil content evaluation of lacustrine organic-rich shales: Methods and a novel quantitative evaluation model. Earth-Science Reviews, 214, 103545.

Hu T., Wu G.Y., Xu Z., Pang X.Q., Liu Y., Yu S., 2022a. Potential resources of conventional, tight, and shale oil and gas from Paleogene Wenchang Formation source rocks in the Huizhou Depression. Advances in Geo-Energy Research, 6, 402-414.

Hu T., Pang X.Q., Xu T.W., Li C.R., Jiang S., Wang Q.F., Chen Y.Y., Zhang H.A., Huang C., Gong S.Y., Gao Z.C., 2022b. Identifying the key source rocks in heterogeneous saline lacustrine shales: Paleogene shales in the Dongpu depression, Bohai Bay Basin, eastern China. AAPG Bulletin, 106.

Hu T., Pang X.Q., Jiang F.J., Zhang C.X., Wu G.Y., Hu M.L., Jiang L., Wang Q.F., Xu T.W., Hu Y., Jiang S., Wang W.Y., Li M.W., 2022c. Dynamic continuous hydrocarbon accumulation (DCHA): Existing theories and a new unified accumulation model. Earth-Science Reviews, 232, 104109.

Huang R.D., Jiang F.J., Chen D., Qiu R.Y., Hu T., Fang L.H., Hu M.L., Wu G.Y., Zhang C.X., Lv J.H., Wu Y.P., Huang L.L., 2023. Astrochronology and carbon-isotope stratigraphy of the Fengcheng Formation, Junggar Basin: Terrestrial evidence for the Carboniferous-Permian Boundary. Gondwana Research, 116, 1-11.

Jones B.E., Grant W., 2000. Microbial Diversity and Ecology of Alkaline Environments., 177-190.

Jones B., Manning D.A.C., 1994. Comparison of geochemical indices used for the interpretation of palaeoredox conditions in ancient mudstones. Chemical Geology, 111, 111-129.

Katz B.J., Lin F., 2021. Consideration of the limitations of thermal maturity with respect to vitrinite reflectance, Tmax, and other proxies. AAPG Bulletin, 105, 695-720.

Kodina L.A., Bogacheva M.P., Lyutsarev S.V., 1996. Particulate organic carbon in the Black Sea: Isotopic composition and origin. Geochemistry International, 34, 798-804.
Kump L.R., Arthur M.A., 1999. Interpreting carbon-isotope excursions: carbonates and organic matter. 161, 198.
Lerman A., 1978. Lakes: chemistry, geology, physics.
Li W.W., Cao J., Zhi D.M., Tang Y., He W.J., Wang T.T., Xia L.W., 2021. Controls on shale oil accumulation in alkaline lacustrine settings: Late Paleozoic Fengcheng Formation, northwestern Junggar Basin. Marine and Petroleum Geology, 129, 105107.
Li J.R., Yang Z., Wu S.T., Pan S.Q., 2021. Key issues and development direction of petroleum geology research on source rock strata in China. Advances in Geo-Energy Research, 5, 121-126.
Liu Y., Wang X., Wu K.Y., Chen S.N., Shi Z., Yao W.J., 2019. Late Carboniferous seismic and volcanic record in the northwestern margin of the Junggar Basin: Implication for the tectonic setting of the West Junggar. Gondwana Research, 71, 49-75.
Lu J., Wang Y., Yang M.F., Shao L.Y., Hilton J., 2021. Records of volcanism and organic carbon isotopic composition ($\delta^{13}C_{org}$) linked to changes in atmospheric pCO_2 and climate during the Pennsylvanian icehouse interval. Chemical Geology, 570, 120168.
Lv J.H., Jiang F.J., Hu T., Zhang C.X., Huang R.D., Hu M.L., Xue J., Huang L.L., Wu Y.P., 2023. Control of complex lithofacies on the shale oil potential in ancient alkaline lacustrine basins: The Fengcheng Formation, Mahu Sag, Junggar basin. Geoenergy Science and Engineering, 224, 211501.
Ma L., Zhang Y., Zhang Z.H., Zhang G.L., Wang S.Z., 2020. The geochemical characteristics of the Fengcheng Formation source rocks from the Halaalate area, Junggar Basin, China. Journal of Petroleum Science and Engineering, 184, 106561.
Peng J.W., 2022. What besides redox conditions? Impact of sea-level fluctuations on redox-sensitive trace-element enrichment patterns in marine sediments. Science China Earth Sciences, 65, 1985-2004.
Peters K.E., 1986. Guidelines for evaluating petroleum source rock using programmed pyrolysis. AAPG Bulletin, 70, 318-329.
Pieńkowski G., Hesselbo S.P., Barbacka M., Leng M.J., 2020. Non-marine carbon-isotope stratigraphy of the Triassic-Jurassic transition in the Polish Basin and its relationships to organic carbon preservation, pCO2 and palaeotemperature. Earth-Science Reviews, 210, 103383.
Percival L.M.E., Ruhl M., Hesselbo S.P., Jenkyns H.C., Mather T.A., Whiteside J.H., 2017. Mercury evidence for pulsed volcanism during the end-Triassic mass extinction. Proceedings of the National Academy of Sciences, 114, 7929-7934.
Sarg J.F., Suriamin N., TÌnavsuu-Milkeviciene K., Humphrey J., 2013. Lithofacies, stable isotopic composition, and stratigraphic evolution of microbial and associated carbonates, Green River Formation (Eocene), Piceance Basin, Colorado. AAPG Bulletin, 97, 1937-1966.
Saunders A.D., 2005. Large Igneous Provinces: Origin and Environmental Consequences. Elements 1, 259-263.
Sengor A.M.C., Natalin B., Burtman V., 1993. Evolution of the Altaid Tectonic collage and Palaeozoic Crustal Growth in Eurasia. Nature, 364.
Shevelkova A.N., Sal'Nikov Y.I., Kuz'Mina N.L., Ryabov A., Wilkin R., Barnes H.L., Brantley S., 1996. The size distribution of framboidal pyrite in modern sediments: An indicator of redox conditions. Geochimica Et Cosmochimica Acta, 60.
Su A., Chen H.H., Zhao J.X., Feng Y.X., 2020. Integrated fluid inclusion analysis and petrography constraints on the petroleum system evolution of the central and southern Biyang Sag, Nanxiang Basin, Eastern China. Marine and Petroleum Geology, 118, 104437.
Tang W.B., Zhang Y.Y., Pe-Piper G., Piper D.J.W., Guo Z.J., Li W., 2021a. Permian to early Triassic tectono-sedimentary evolution of the Mahu sag, Junggar Basin, western China: sedimentological implications of the transition from rifting to tectonic inversion. Marine and Petroleum Geology, 123, 104730.
Tang W.B., Zhang Y.Y., Pe-Piper G., Piper D.J.W., Guo Z.J., Li W., 2021b. Permian rifting processes in the NW Junggar Basin, China: Implications for the post-accretionary successor basins. Gondwana Research, 98, 107-124.
Tang Y., Cao J., He W.J., Guo X.G., Zhao K.B., Li W.W., 2021. Discovery of shale oil in alkaline lacustrine basins: The Late Paleozoic Fengcheng Formation, Mahu Sag, Junggar Basin, China. Petroleum Science, 18, 1281-1293.
Tissot B., Welte D., 1984. Petroleum Formation an Occurrence. Springer-Verlag, New York.
Tobin T.S., Honeck J.W., Fendley I.M., Weaver L.N., Sprain C.J., Tuite M.L., Flannery D.T., Mans W.W., Wilson M.G.P., 2021. Analyzing sources of uncertainty in terrestrial organic carbon isotope data: A case study across the K-Pg boundary in Montana, USA. Palaeogeography, Palaeoclimatology, Palaeoecology, 574, 110451.
Tribovillard N., Riboulleau A., Lyons T., Baudin F., 2004. Enhanced trapping of molybdenum by sulfurized marine organic matter of marine origin in Mesozoic limestones and shales. Chemical Geology, 213, 385-401.
Tribovillard N., Algeo T.J., Baudin F., Riboulleau A., 2012. Analysis of marine environmental conditions based onmolybdenum–uranium covariation—Applications to Mesozoic paleoceanography. Chemical Geology, 324-325, 46-58.
Tyson R., 1995. Sedimentary Organic Matter: Organic Facies and Palynofacies, pp.1-6.
Wan Y., Feng Q., Liu Y., Tabor N., Dan M., Crowley J.L., Lin J., Thomas S., 2010. Depositional environments and cyclo- and chronostratigraphy of uppermost Carboniferous-Lower Triassic fluvial–lacustrine deposits, southern Bogda Mountains, NW China - A terrestrial paleoclimatic record of mid-latitude NE Pangea. Global and Planetary Change, 73, 15-113.
Wang Q.F., Jiang F.J., Ji H.C., Jiang S., Guo F.X., Gong S.Y., Wang Z., Liu X.H., Li B.S., Chen Y.Y., Deng Q., 2020. Differential Enrichment of Organic Matter in Saline Lacustrine Source Rocks in a Rift Basin: A Case Study of Paleogene Source Rocks, Dongpu Depression, Bohai Bay Basin. Natural Resources Research 29, 4053-4072.
Wang T.T., Cao J., Jin J., Xia L.W., Xiang B.L., Ma W.Y., Li W.W., He W.J., 2021. Spatiotemporal evolution of a Late Paleozoic alkaline lake in the Junggar Basin, China. Marine and Petroleum Geology, 124, 104799.
Wang T.T., Cao J., Xia L., Zhi D.M., Tang Y., He W.J., 2022. Revised age of the Fengcheng Formation, Junggar Basin, China: Global implications for the late Paleozoic ice age. Global and Planetary Change 208, 103725.
Wei W., Algeo T.J., 2020. Elemental proxies for paleosalinity analysis of ancient shales and mudrocks. Geochimica Et Cosmochimica Acta, 287, 341-366.
White A.H., Youngs B.C., 1980. Cambrian Alkali Playa-Lacustrine Sequence in the Northeastern Officer Basin, South Australia. Journal of Sedimentary Petrology, 50, 1279-1286.
Wilkin R.T., Barnes H.L., Brantley S.L., 1996. The size distribution of framboidal pyrite in modern sediments: An indicator of redox conditions. Geochimica Et Cosmochimica Acta, 60, 3897-3912.

Yang Z., Zou C.N., Hou L.H., Wu S.T., Lin S.H., Luo X., Zhang L.J., Zhao Z.Y., Cui J.W., Pan S.Q., 2019. Division of fine-grained rocks and selection of "sweet sections" in the oldest continental shale in China: Taking the coexisting combination of tight and shale oil in the Permian Junggar Basin. Marine and Petroleum Geology, 109, 339-348.
Yu K.H., Cao Y.C., Qiu L.W., Sun P.P., Jia X.Y., Wan M., 2018. Geochemical characteristics and origin of sodium carbonates in a closed alkaline basin: The Lower Permian Fengcheng Formation in the Mahu Sag, northwestern Junggar Basin, China. Palaeogeography, Palaeoclimatology, Palaeoecology, 511, 506-531.
Zhang B.L., Yao S.P., Mills B.J.W., Wignall P.B., Hu W.X., Liu B., Ren Y.L., Li L.L., Shi G., 2020. Middle Permian organic carbon isotope stratigraphy and the origin of the Kamura Event. Gondwana Research, 79, 217-232.
Zhang Z.L., Wu L.Y., Shu N.Z., 2006. Cause analysis of abnormal Tmax values on Rock-Eval purolysis. Petroleum Exploration and Development, 72-75.
Zhi D.M., Song Y., He W.J., Jia X.Y., Zou Y., Huang L.L., 2019. Geological characteristics, resource potential and exploration direction of shale oil in Middle-Lower Permian, Junggar Basin. Xinjiang Petroleum Geology, 40, 389-401.
Zhi D.M., Tang Y., He W.J., Guo X.G., Zheng M.L., Huang L.L., 2021. Orderly coexistence and accumulation models of conventional and unconventional hydrocarbons in Lower Permian Fengcheng Formation, Mahu sag, Junggar Basin. Petroleum Exploration and Development, 48, 43-59.
Zhou C.M., Jiang S.Y., 2009. Palaeoceanographic redox environments for the lower Cambrian Hetang Formation in South China: Evidence from pyrite framboids, redox sensitive trace elements, and sponge biota occurrence. Palaeogeography Palaeoclimatology Palaeoecology - Palaeogeogr Palaeoclimatol, 271, 279-286.

About the first author

HUANG Renda, male, born in 1999; Master; graduated from China University of Petroleum (Beijing). His current research interest is shale oil accumulation.

About the correspondence author

JIANG Fujie, male, born in 1979 in Lanxi City, Heilongjiang Province; PhD; graduated from the Chinese University of Petroleum (Beijing); Professor at China University of Petroleum (Beijing). He is interested in organic matter enrichment mechanism and regional carbon cycle response, as well as shale oil enrichment geological conditions.

Figures and Captions

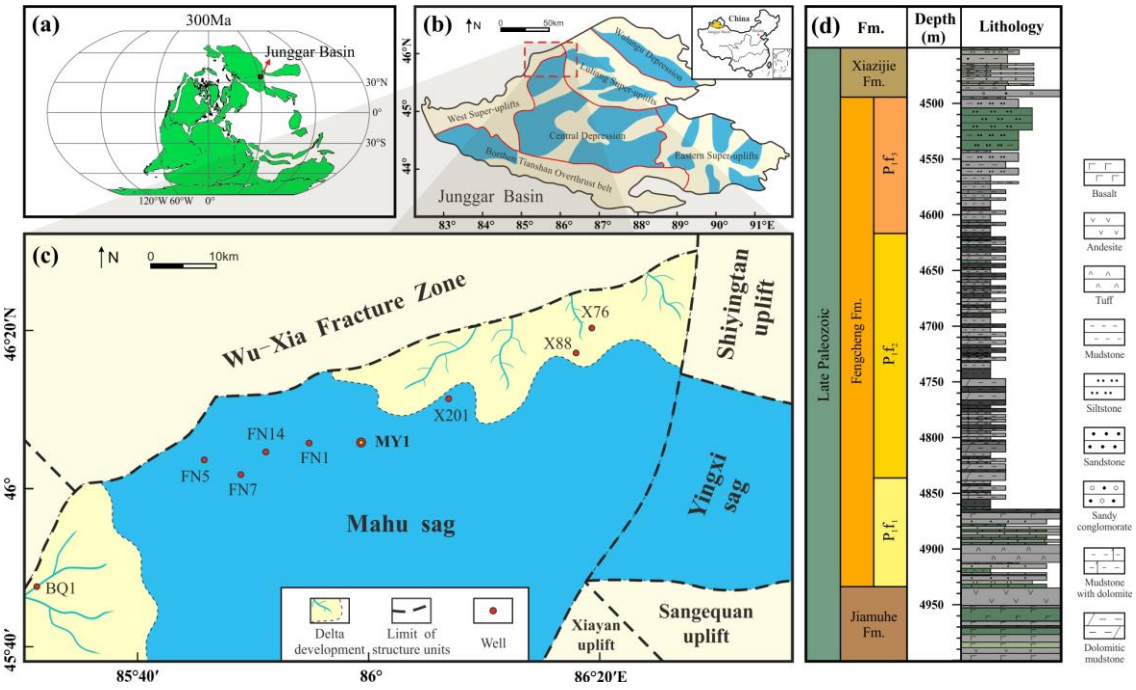

Fig. 1. Overview of study area and lithology of Fengcheng Formation, MY1.
(a) The location of Junggar Basin at ca. 300Ma shown by Paleogeographic map, modified from https://portal.gplates.org/. (b) The location of Mahu Sag in Junggar Basin (China basemap after China National Bureau of Surveying and Mapping Geographical Information). (c) Mahu Sag structural division, modified from CNPC Xinjiang oilfield. (d) Stratigraphy and lithology of MY1.

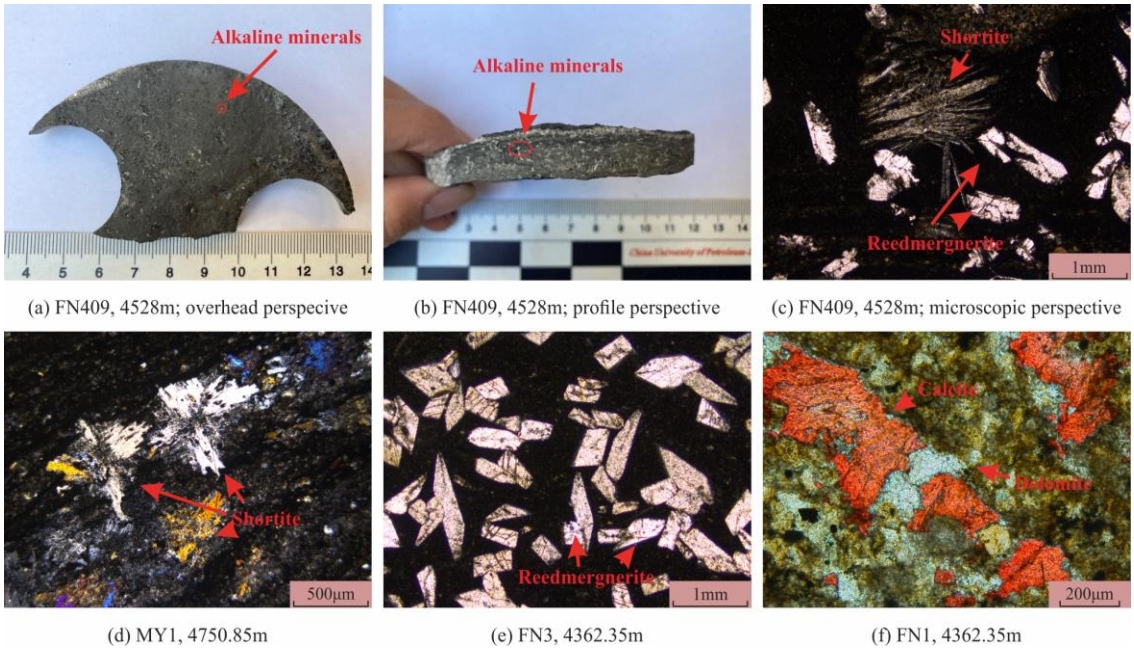

Fig. 2. Characteristics of alkaline minerals in Fengcheng Formation.

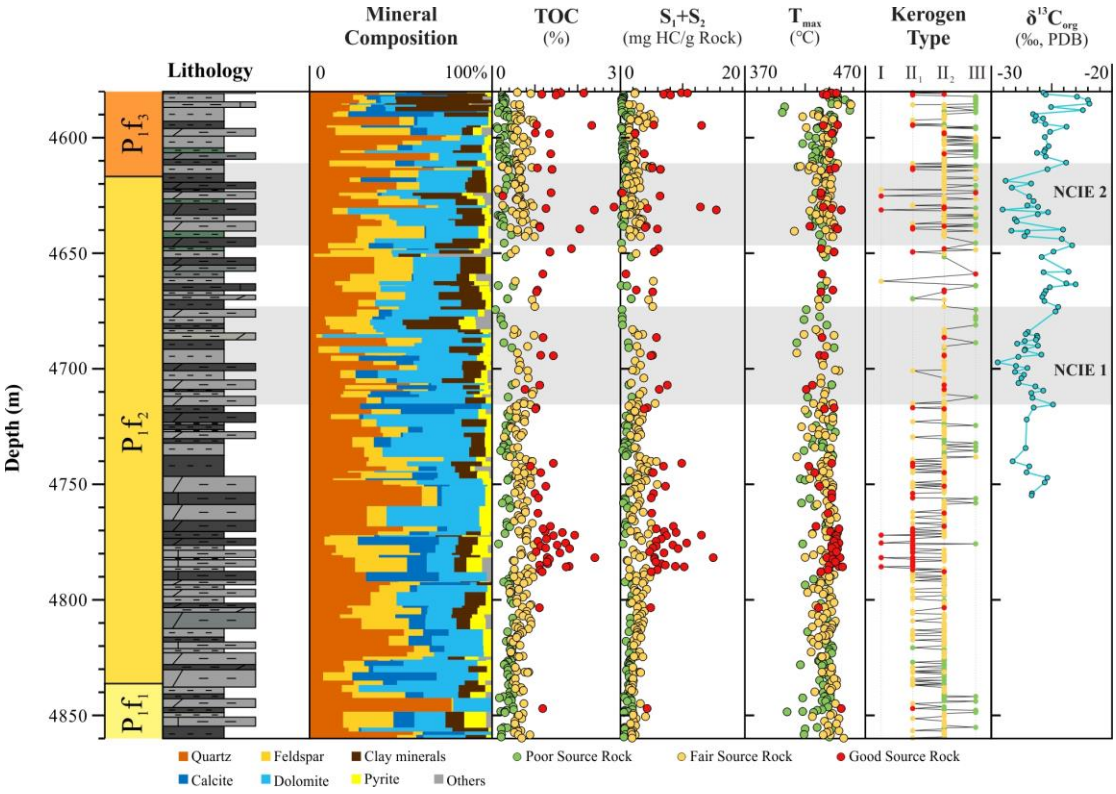

Fig. 3. Stratigraphic division, lithology, mineral composition, and source rock parameters of the LPF shale, MY1. The two gray shaded areas represent the two NCIEs, while the lower one is NCIE 1, and the upper one is NCIE 2.

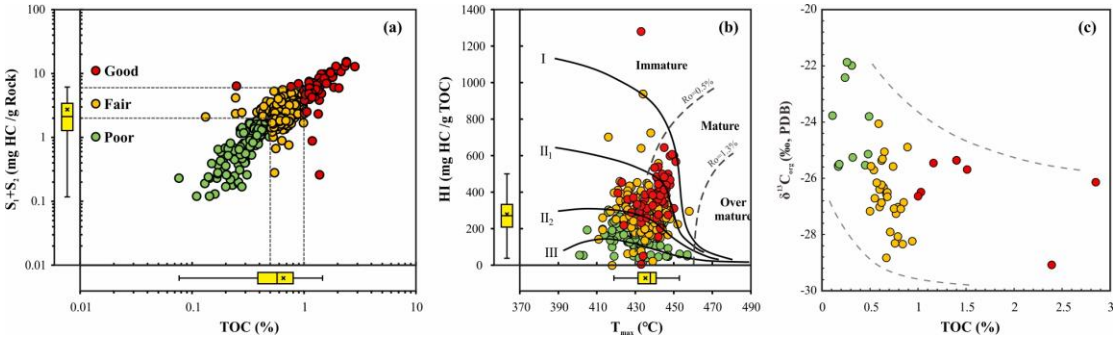

Fig. 4. (a) S_1+S_2 verse TOC plot showing the OM abundance of the LPF shale, MY1. The green, yellow, and red points represent poor source rock, fair source rock, and good source rock, respectively. (b) HI verse Tmax plot showing the kerogen types of the LPF shale. (c) $\delta^{13}C_{org}$ verse TOC showing their negative correlation.

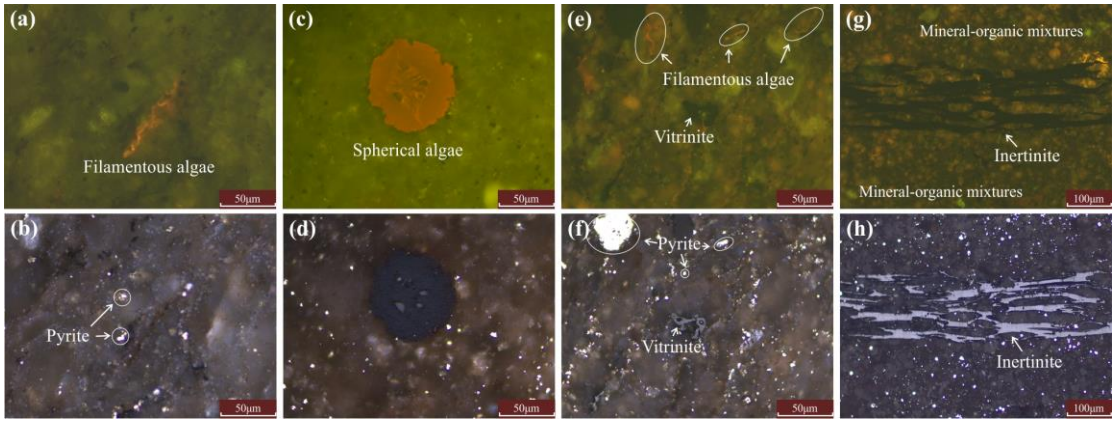

Fig. 5. Typical macerals of the LPF shale in Mahu sag.
(a-b) MY1 4742.16m, TOC=0.89%, type II_1. (c-d) MY1 4807.89m, TOC=0.86%, type II_2. (e-f) MY1 4750.82m, TOC=1.25%, type II_2. (g-h) MY1 4709.64m, TOC=0.97%, type II_2. The left and right are the same field under fluorescent light and reflected light.

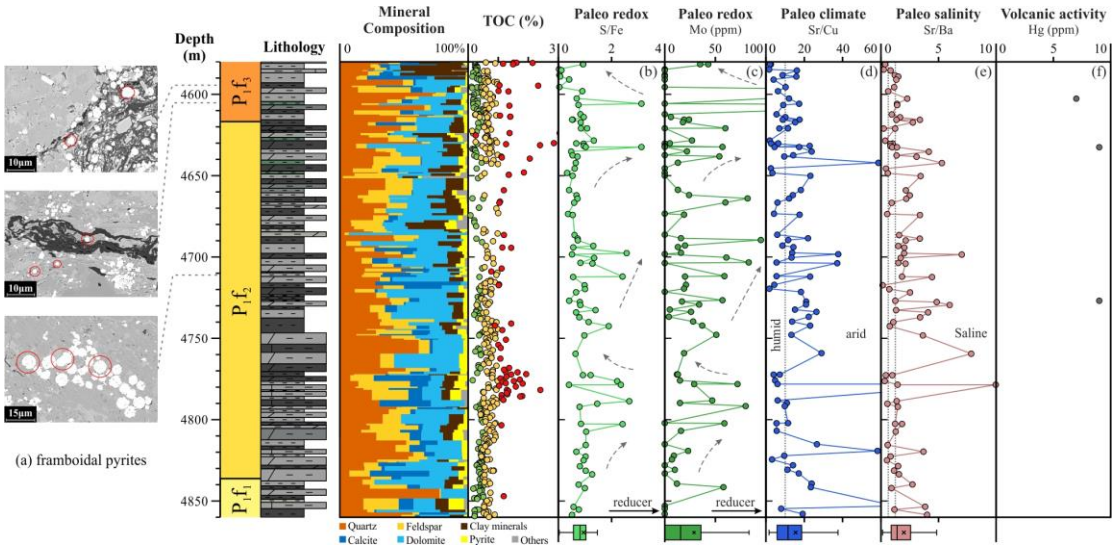

Fig. 6. Variations of geochemical proxies in the LPF shale, MY1.
(a) Framboidal pyrites. White overexposed minerals in the SEM image are pyrite, mostly in the form of framboids and aggregates. (b) S/Fe of the LPF shale. The larger the value, the more reductive the environment is (Dean and Arthur, 1989; Peng, 2022). (c) Mo concentrations of the LPF shale. (d) Sr/Cu of the LPF shale indicates the paleo climate of the LPF shale. Sr/Cu<10 indicates humid climate, while Sr/Cu>10 indicates arid climate (Lerman, 1978). (e) Sr/Ba variations of the LPF shale. Sr/Ba<0.5, 0.5< Sr/Ba<1, and Sr/Ba>1 indicates the fresh, brackish, and saline lacustrine environment, respectively (Chivas et al., 1985). (f) Hg concentration of the LPF shale.

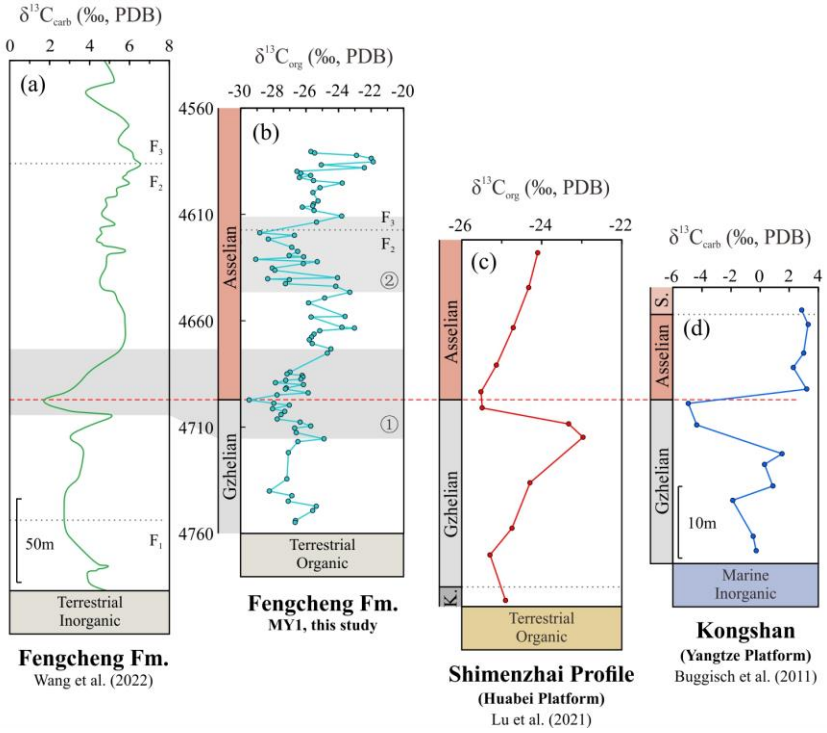

Fig. 7. Global $\delta^{13}C$ profiles comparison.
(a) Fengcheng Formation integrated $\delta^{13}C_{carb}$ profile, modified from Wang et al. (2022). (b) Fengcheng Formation $\delta^{13}C_{org}$ profile in MY1, this study. The stratigraphic correlation is from Huang et al. (2023). (c) Terrestrial Shimenzhai $\delta^{13}C_{org}$ profile, Huabei Platform, modified from Lu et al. (2021). (d) Marine Kongshan $\delta^{13}C_{carb}$ profile, Yangtze Platform, modified from Buggisch et al. (2011). K. Kasimovian; S. Sakmarian.

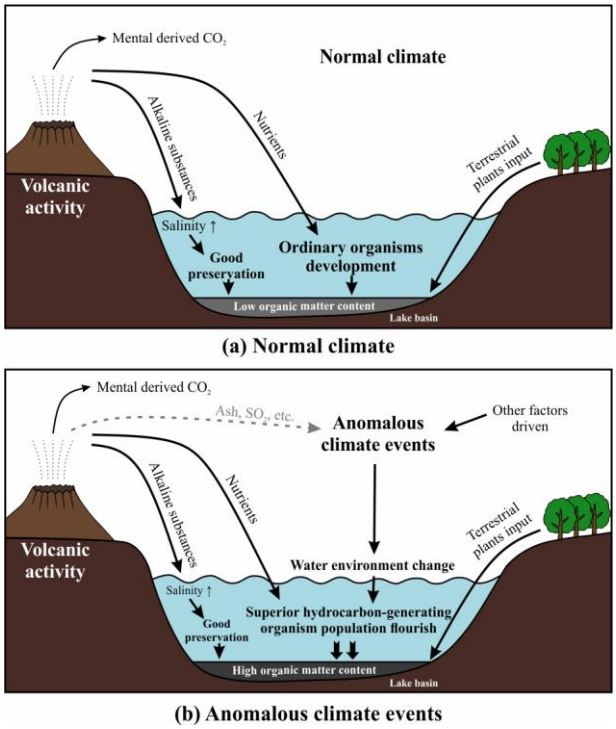

Fig. 8. Different enrichment processes of organic matters of the LPF alkaline lake source rocks.
(a) Organic matter enrichment process under normal climate. (b) Organic matter enrichment process under anomalous climate events.